
Figures and figure supplements

cAMP–EPAC–PKC ϵ –RIM1 α signaling regulates presynaptic long-term potentiation and motor learning

Xin-Tai Wang, Lin Zhou and Bin-Bin Dong *et al.*

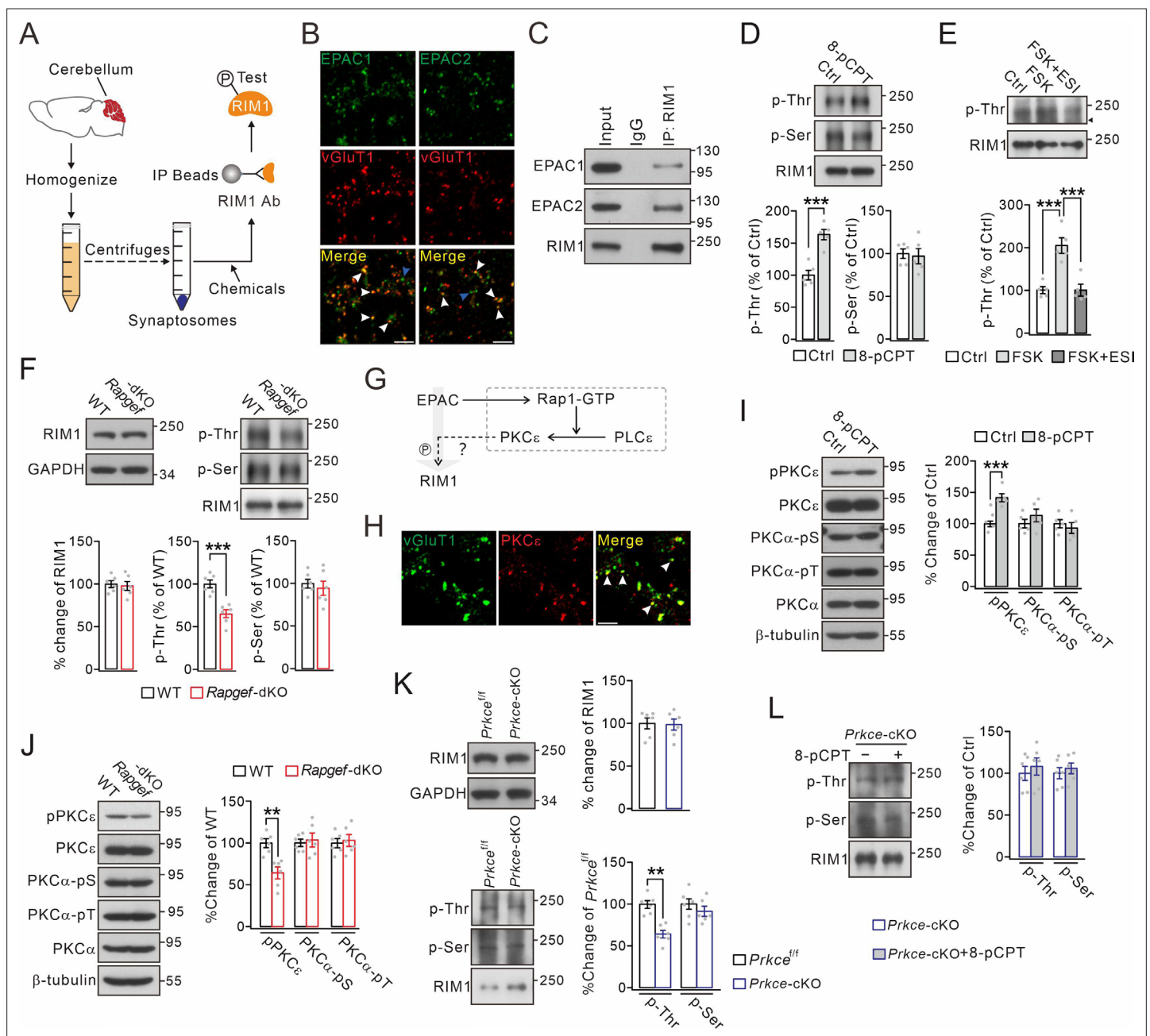


Figure 1. Threonine phosphorylation of RIM1 by EPAC and PKC ϵ . **(A)** Schematic showing purification of cerebellar synaptosomes and phosphorylation assay of RIM1. **(B)** Immunostaining of EPAC1 or EPAC2 along with vGluT1 (white arrowheads) in cerebellar synaptosomes. Blue arrowheads show the synaptosomes marked by only EPAC1 or EPAC2. Scale bars, 5 μ m. **(C)** Precleared synaptosomes (WT) were immunoprecipitated with anti-RIM1 antibody and probed with antibodies to EPAC1, EPAC2 and RIM1. Rabbit IgG was negative control. $n=4$. **(D)** WT synaptosomes were treated with control buffer (Ctrl) or 8-pCPT (20 μ M, 30 min) and p-Thr and p-Ser of RIM1 were analyzed. p-Thr and p-Ser were normalized to corresponding RIM1 and percentage changes relative to Ctrl are plotted. p-Thr: $100 \pm 8\%$ (Ctrl) and $163 \pm 8\%$ (8-pCPT; $p=0.00043$). p-Ser: $100 \pm 6\%$ (Ctrl) and $97 \pm 9\%$ (8-pCPT; $p=0.77$). Unpaired t test. $n=5$ for all groups. *** $p<0.001$. **(E)** p-Thr and p-Ser of RIM1 in WT synaptosomes treated with control buffer, forskolin (FSK; 20 μ M, 30 min), or FSK + ESI-09 (50 μ M, 30 min) (FSK + ESI). Arrowhead marks nonspecific protein. p-Thr: $100 \pm 8\%$ (Ctrl), $205 \pm 18\%$ (FSK; $p<0.001$ vs. Ctrl), and $101 \pm 14\%$ (FSK + ESI; $p=0.98$ vs. Ctrl; $p<0.001$ vs. FSK). One-way ANOVA test. $n=5$ for all groups. *** $p<0.001$. **(F)** Phosphorylation of synaptosomal RIM1 from WT and *Rapgef3/4*-dKO mice. RIM1: $100 \pm 4\%$ (WT) and $98 \pm 5\%$ (*Rapgef3/4*-dKO; $p=0.72$). p-Thr: $100 \pm 5\%$ (WT) and $65 \pm 5\%$ (*Rapgef3/4*-dKO; $p=0.00032$). p-Ser: $100 \pm 5\%$ (WT) and $94 \pm 8\%$ (*Rapgef3/4*-dKO; $p=0.57$). Unpaired t test. $n=6$ for all groups. *** $p<0.001$. **(G)** Schematic depiction of proposed working model. The solid lines show known signaling pathways and the dashed line shows the hypothesis. **(H)** Immunostaining of PKC ϵ and vGluT1 (arrowheads) in cerebellar synaptosomes. Scale bar, 5 μ m. **(I)** WT synaptosomes were treated with control buffer or 8-pCPT (20 μ M, 30 min). The phosphorylations of PKC ϵ and PKC α were normalized to β -tubulin and percentage changes relative to control are plotted. pPKC ϵ : $100 \pm 5\%$ (Ctrl)

Figure 1 continued on next page

Figure 1 continued

and $142 \pm 7\%$ (8-pCPT; $p=0.0007$). PKC α -pSer: $100 \pm 8\%$ (Ctrl) and $113 \pm 11\%$ (8-pCPT; $p=0.31$). PKC α -pThr: $100 \pm 7\%$ (Ctrl) and $93 \pm 10\%$ (8-pCPT; $p=0.54$). Unpaired *t* test. $n=5$ for all groups. *** $p<0.001$. (J) Phosphorylation of synaptosomal PKC ϵ and PKC α in WT and *Rapgef3/4*-dKO mice. pPKC ϵ , PKC α -pSer and PKC α -pThr were normalized to β -tubulin and their percentage changes relative to WT are plotted. pPKC ϵ : $100 \pm 5\%$ (WT) and $64 \pm 7\%$ (*Rapgef3/4*-dKO; $p=0.0013$). PKC α -pSer: $100 \pm 4\%$ (WT) and $103 \pm 8\%$ (*Rapgef3/4*-dKO; $p=0.70$). PKC α -pThr: $100 \pm 6\%$ (WT) and $103 \pm 7\%$ (*Rapgef3/4*-dKO; $p=0.73$). Unpaired *t* test. $n=6$ for all groups. ** $p<0.01$. (K) Phosphorylation of synaptosomal RIM1 in *Prkce*^{fl/fl} and *Prkce*-cKO mice. RIM1: $100 \pm 6\%$ (WT) and $99 \pm 6\%$ (*Rapgef3/4*-dKO; $p=0.88$). p-Thr: $100 \pm 3\%$ (*Prkce*^{fl/fl}) and $65 \pm 6\%$ (*Prkce*-cKO; $p=0.0028$). p-Ser: $100 \pm 5\%$ (*Prkce*^{fl/fl}) and $95 \pm 9\%$ (*Prkce*-cKO; $p=0.57$). Unpaired *t* test. $n=6$ for all groups. ** $p<0.01$. (L) Synaptosomes (*Prkce*-cKO) were treated wi/wo 8-pCPT (20 μ M, 30 min) and RIM1 phosphorylation was analyzed. p-Thr: $100 \pm 8\%$ (*Prkce*-cKO) and $108 \pm 10\%$ (*Prkce*-cKO +8 pCPT; $p=0.55$). p-Ser: $100 \pm 7\%$ (*Prkce*-cKO) and $106 \pm 6\%$ (*Prkce*-cKO +8 pCPT; $p=0.57$). Unpaired *t* test. $n=6$ for all groups. See the online **Figure 1—source data 1** file for source data of western blots in this figure.

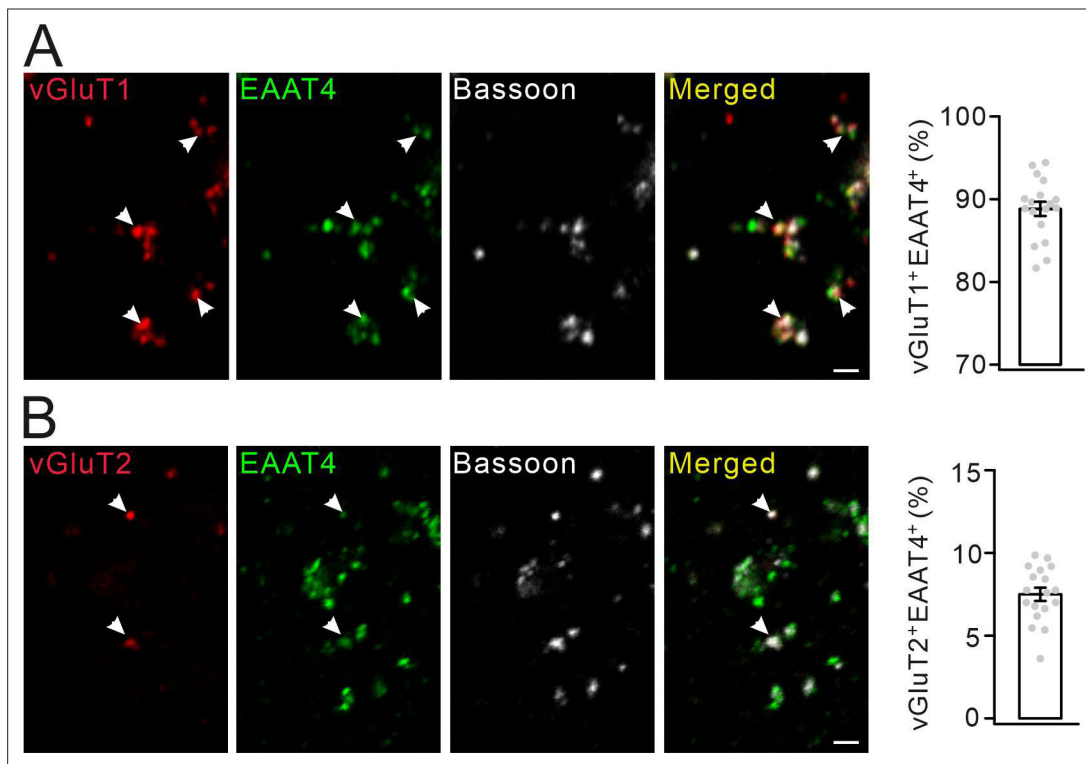


Figure 1—figure supplement 1. The percentages of PF and CF synapses among cerebellar synaptosomes. **(A)** Immunostaining of vGluT1, EAAT4 and Bassoon in cerebellar synaptosomes. White arrowheads show PF synapse simultaneously marked by vGluT1 and EAAT4. Scale bar, 2 μm. Averaged percentage of PF synapses: $88.8 \pm 0.8\%$. **(B)** Immunostaining of vGluT2, EAAT4 and Bassoon in cerebellar synaptosomes. White arrowheads show CF synapse simultaneously marked by vGluT2 and EAAT4. Scale bar, 2 μm. Averaged percentage of CF synapses: $7.5 \pm 0.4\%$.

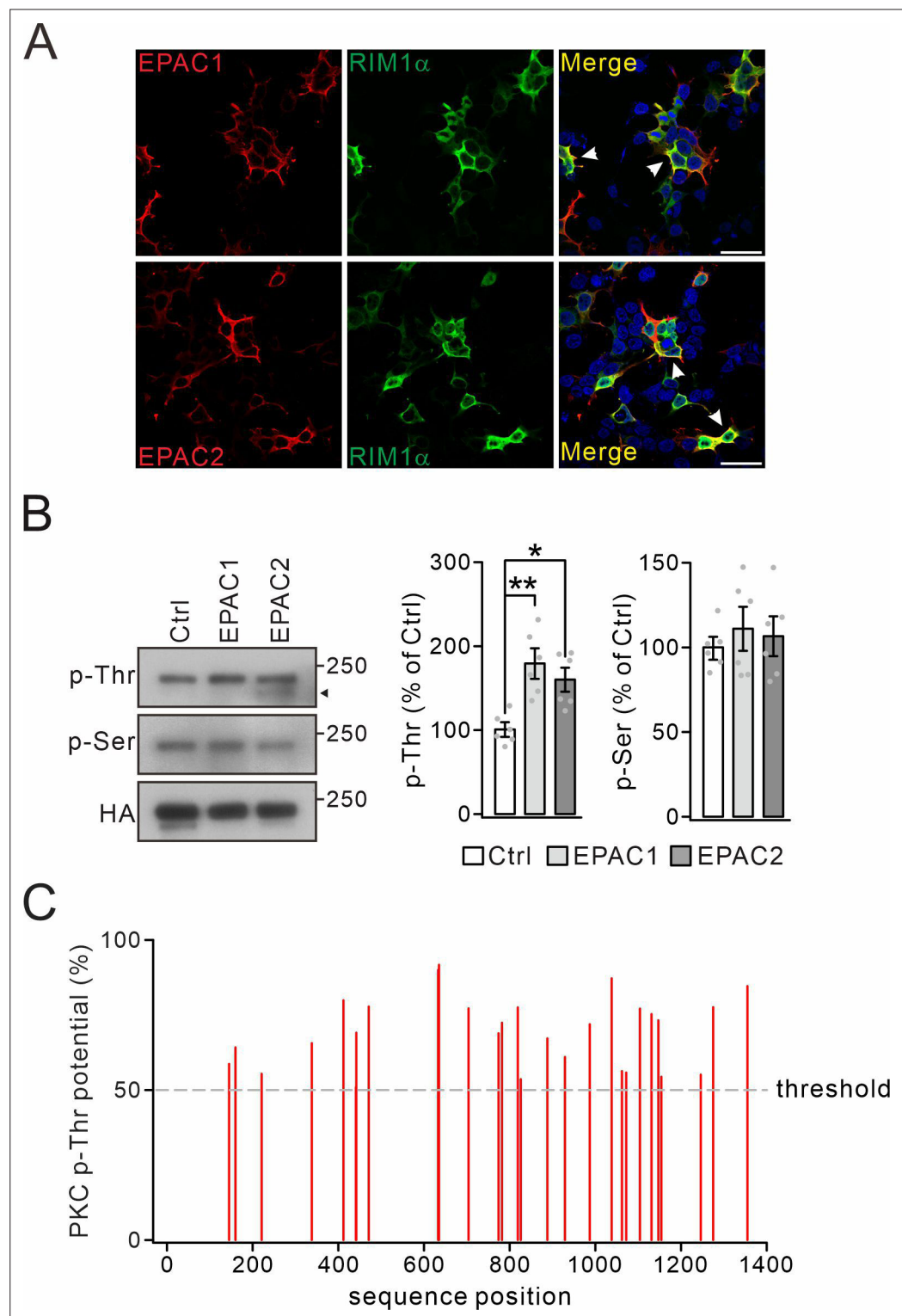


Figure 1—figure supplement 2. Threonine phosphorylation of RIM1 by EPAC in vitro. **(A)** Co-transfection of HA-RIM1α with Flag-EPAC1 or Flag-EPAC2 in HEK cells. Arrowheads show the co-localization of RIM1α and EPACs. Scale bars: 100 μm. **(B)** HA-RIM1α (Ctrl) or HA-RIM1α with Flag-EPACs was transfected into HEK cells and p-Thr and p-Ser of RIM1α were measured. Arrowhead marks non-RIM1 protein. p-Thr: 100 ± 7 (Ctrl), 179 ± 17% (EPAC1; $p=0.0011$ vs. Ctrl), and 160 ± 13% (EPAC2; $p=0.010$ vs. Ctrl). p-Ser: 100 ± 5 (Ctrl), 111 ± 12% (EPAC1; $p=0.69$ vs. Ctrl), and 107 ± 10% (EPAC2; $p=0.87$ vs. Ctrl). One-way ANOVA test. $n=6$ for all groups. * $p<0.05$. ** $p<0.01$. **(C)** Potential threonine phosphorylation sites by PKC in RIM1α were determined using the NetPhos 3.1 server (Technical

Figure 1—figure supplement 2 continued on next page

Figure 1—figure supplement 2 continued

University of Denmark; <http://www.cbs.dtu.dk/services/NetPhos/>). Dashed line: threshold for phosphorylation potential. See the online **Figure 1—figure supplement 2—source data 1** or source data of western blots in this figure.

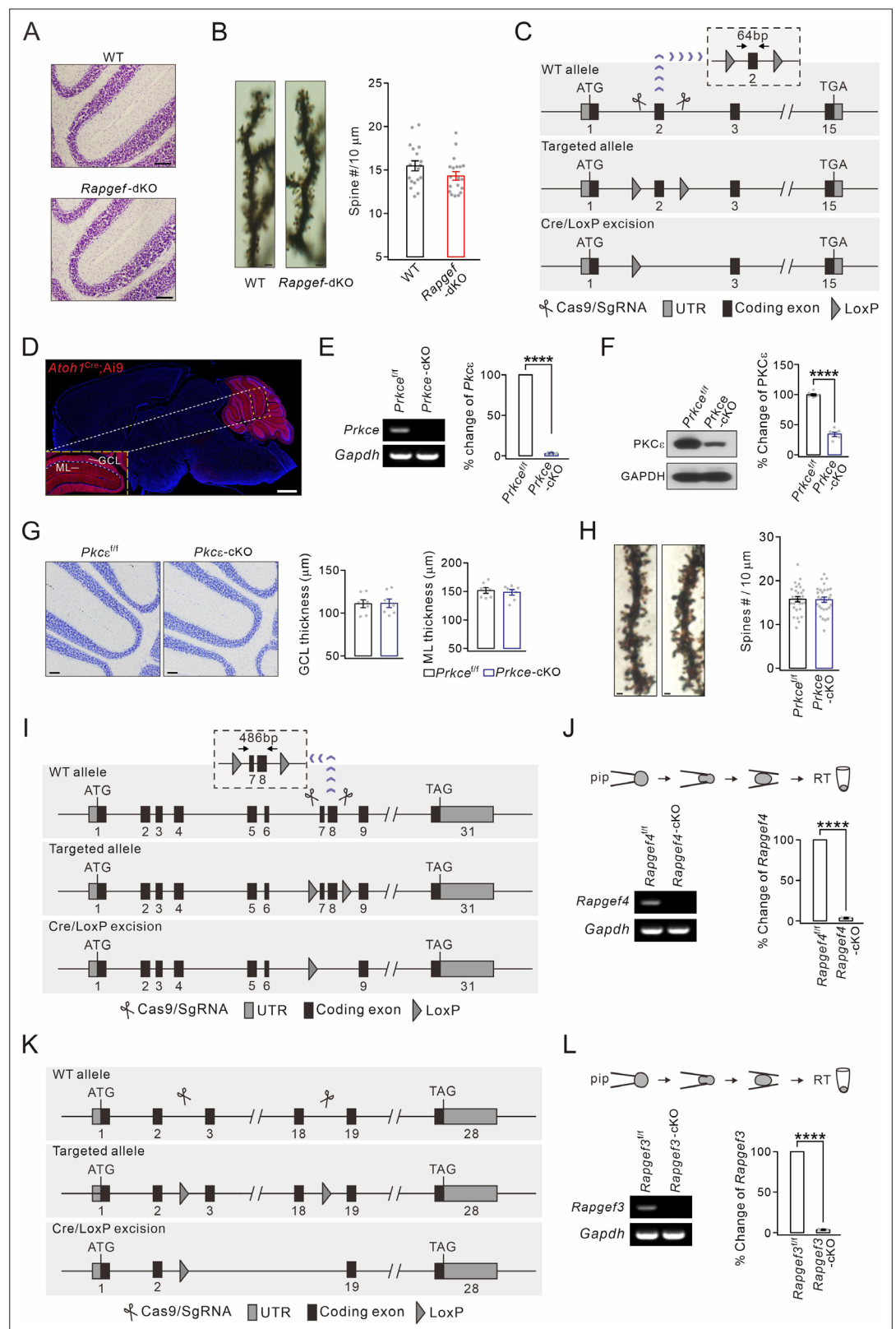


Figure 1—figure supplement 3. Generation of *Prkce*-cKO and *Rapgef3*/*Rapgef4*-cKO mice and cerebellar cytology. **(A)** Nissl staining in the cerebellum from WT and *Rapgef3*-dKO mice. Scale bars, 100 μ m. **(B)** Golgi staining showing apical PC spines. Scale bars, 2 μ m. Average numbers of spines per 10 μ m were 15.5 ± 0.6 (WT; $n=19$ cells) and 14.3 ± 0.5 (*Rapgef3*-dKO; $n=19$ cells). $p=0.13$. Unpaired t test. **(C)** The construction of *Prkce*^{fl/fl} mice. Figure 1—figure supplement 3 continued on next page

Figure 1—figure supplement 3 continued

LoxP sites were inserted before and after exon 2 and further excised by *Atoh1^{Cre}*. **(D)** Native tdTomato fluorescence in the brain of *Atoh1^{Cre};Ai9* mouse. Scale bars: 1 mm. **(E)** Granule cell contents of *Prkce^{fl/fl}* and *Prkce*-cKO mice were harvested using glass micropipettes and subjected to RT-PCR. *Prkce* (165 bp) was absent in *Prkce*-cKO granule cells. *****p*<0.0001. **(F)** PKC ϵ expression in the cerebellum from *Prkce^{fl/fl}* and *Prkce*-cKO mice. Percentage changes of PKC ϵ : $100 \pm 2\%$ (*Prkce^{fl/fl}*; *n*=6) and $34 \pm 4\%$ (*Prkce*-cKO; *n*=6). Unpaired *t* test. *****p*<0.001. **(G)** Nissl staining in the cerebellum. Scale bars, 100 μ m. GCL thickness: $111.0 \pm 4.9 \mu$ m (*Prkce^{fl/fl}*) and $111.6 \pm 5.4 \mu$ m (*Prkce*-cKO), *p*=0.93, unpaired *t* test. ML thickness: $151.7 \pm 5.3 \mu$ m (*Prkce^{fl/fl}*) and $148.4 \pm 5.3 \mu$ m (*Prkce*-cKO), *p*=0.64, unpaired *t* test. *n*=7 for all groups. **(H)** Golgi staining showing apical PC spines in *Prkce^{fl/fl}* and *Prkce*-cKO mice. Scale bars, 2 μ m. Average numbers of spines per 10 μ m: 15.8 ± 0.6 (*Prkce^{fl/fl}*; *n*=29 cells) and 15.7 ± 0.6 (*Prkce*-cKO; *n*=28 cells), *p*=0.88, unpaired *t* test. **(I)** The construction of *Rapgef4^{fl/fl}* mice. LoxP sites were inserted between exons 6 and 9 and further excised by *Atoh1^{Cre}*. **(J)** Granule cell contents of *Rapgef4^{fl/fl}* and *Rapgef4*-cKO mice were harvested and subjected to RT-PCR. *Rapgef4* (180 bp) was absent in *Rapgef4*-cKO granule cells. *****p*<0.001. **(K)** The construction of *Rapgef3^{fl/fl}* mice. LoxP sites were inserted between exons 3 and 18 and further excised by *Atoh1^{Cre}*. **(L)** Granule cell contents of *Rapgef3^{fl/fl}* and *Rapgef3*-cKO mice were harvested and subjected to RT-PCR. *Rapgef3* (218 bp) was absent in *Rapgef3*-cKO granule cells. *****p*<0.001. See the online **Figure 1—figure supplement 3—source data 1** file for source data of western blots in this figure.

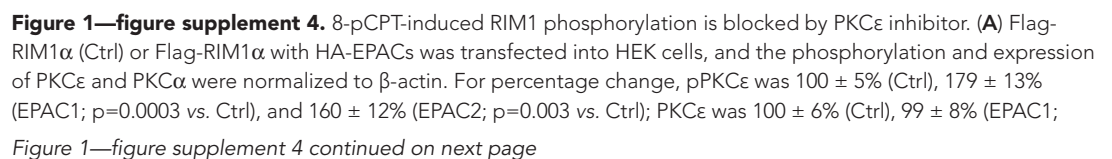


Figure 1—figure supplement 4 continued

p=0.96 vs. Ctrl), and $101 \pm 8\%$ (EPAC2; p=0.92 vs. Ctrl); PKC α -pS was $100 \pm 7\%$ (Ctrl), $101 \pm 10\%$ (EPAC1; p=0.94 vs. Ctrl), and $96 \pm 8\%$ (EPAC2; p=0.67 vs. Ctrl); and PKC α -pT was $100 \pm 6\%$ (Ctrl), $97 \pm 10\%$ (EPAC1; p=0.81 vs. Ctrl), and $101 \pm 8\%$ (EPAC2; p=0.90 vs. Ctrl). One-way ANOVA test. n=6 for all groups. **p<0.01. ***p<0.001.

(B) Precleared synaptosomes from WT mice were immunoprecipitated with anti-RIM1 antibody and probed with antibodies to PKC ϵ and RIM1. n=4. **(C)** HA-RIM1 α (Ctrl) or HA-RIM1 α with His-PKC ϵ was transfected into HEK cells and p-Thr and p-Ser of RIM1 α were analyzed. p-Thr and p-Ser were normalized to HA and percentage changes relative to Ctrl are plotted. p-Thr was $100 \pm 8\%$ (Ctrl) and $179 \pm 18\%$ (PKC ϵ ; p=0.0021). p-Ser was $100 \pm 11\%$ (Ctrl) and $118 \pm 13\%$ (PKC ϵ ; p=0.26). n=5 for all groups. Unpaired t test. **p<0.01. **(D)** Synaptosomes (WT) were treated with control buffer, 8-pCPT (20 μ M, 30 min), 8-pCPT+ ϵ V1-2 (5 μ M, 30 min) and 8-pCPT+Gö (10 μ M, 30 min). p-Thr was normalized to RIM1 and percentage changes relative to Ctrl are plotted. Ctrl: $100 \pm 8\%$. 8-pCPT: $280 \pm 35\%$ (p=0.0016 vs. Ctrl). 8-pCPT+ ϵ V1-2: $147 \pm 19\%$ (p=0.58 vs. Ctrl; p=0.015 vs 8-pCPT). 8-pCPT+Gö: 276 ± 31 (p=0.0019 vs. Ctrl; p=0.99 vs 8-pCPT; p=0.017 vs 8-pCPT+ ϵ V1-2). One-way ANOVA test. n=4 for all groups. *p<0.05. **p<0.01. **(E)** Synaptosomes (WT) were treated with control buffer, PMA (1 μ M, 30 min), PMA+ ϵ V1-2 (5 μ M, 30 min) and PMA +Gö (10 μ M, 30 min). RIM1 p-Thr was normalized to RIM1, and percentage changes relative to Ctrl are plotted. Ctrl: $100 \pm 8\%$. PMA: $208 \pm 19\%$ (p=0.0041 vs. Ctrl). PMA+ ϵ V1-2: $134 \pm 13\%$ (p=0.55 vs. Ctrl; p=0.043 vs. PMA). PMA +Gö: $214 \pm 24\%$ (p=0.0029 vs. Ctrl; p=0.99 vs. PMA; p=0.030 vs. PMA+ ϵ V1-2). One-way ANOVA test. n=4 for all groups. *p<0.05. **p<0.01. See the online **Figure 1—figure supplement 4—source data 1** file for source data of western blots in this figure.

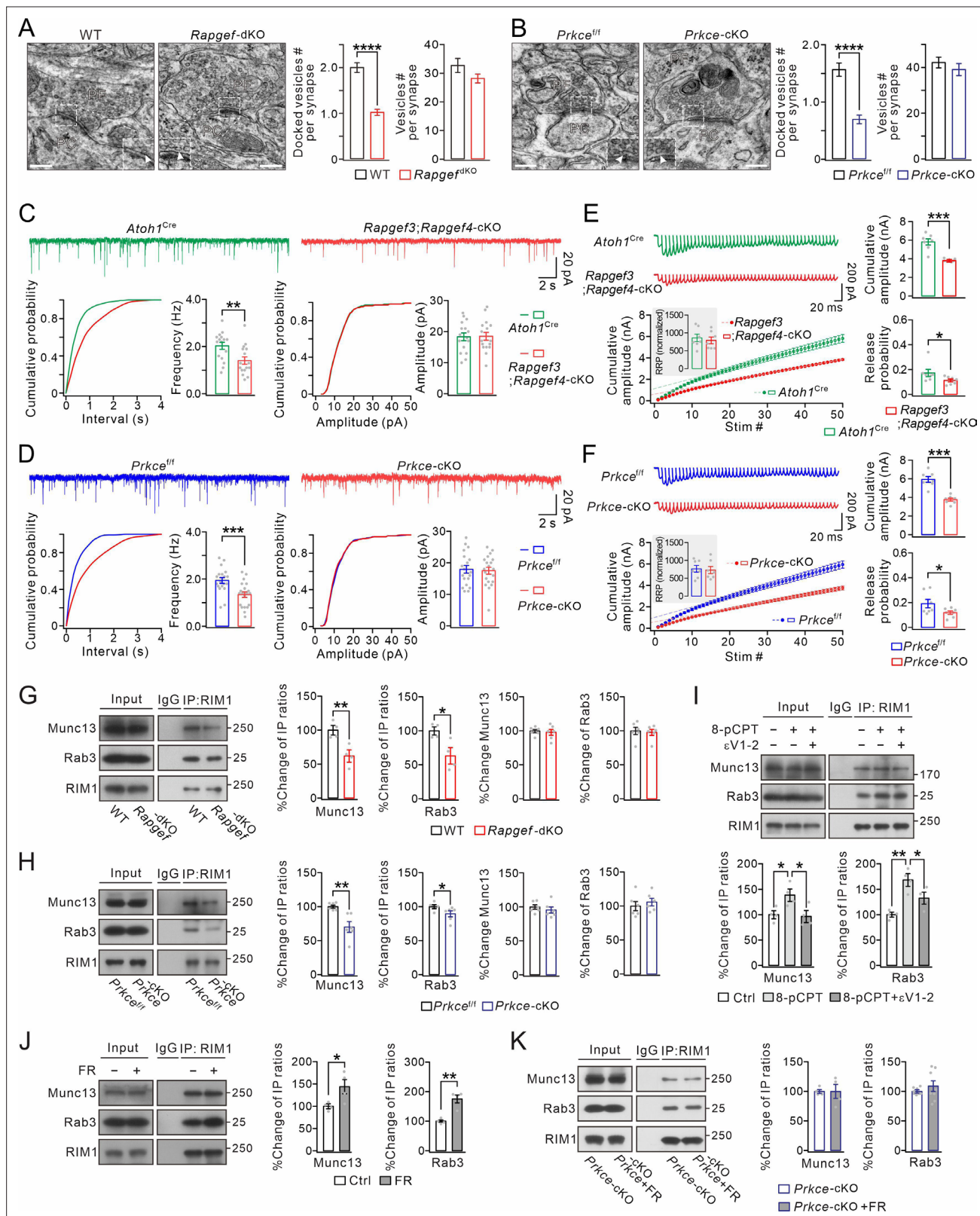


Figure 2. EPAC and PKCε act on vesicle docking, synaptic release, and Rab3-RIM1-Munc13 complex. **(A)** Representative EM (23,000×) of PF-PC synapses of WT and *Rapgef3/4*-dKO mice. Scale bars: 200 nm. The inserts show docked vesicles. Unpaired t test. ****p<0.0001. **(B)** Representative EM of PF-PC synapses of *Prkce*^{fl/fl} and *Prkce*-cKO mice. Scale bars: 200 nm. Unpaired t test. ****p<0.0001. **(C)** Example PC mEPSCs in *Atoh1*^{Cre} and *Rapgef3*;*Rapgef4*-cKO mice. Lower: statistics of inter-event interval and amplitude. Grey dots indicate individual data points. Frequency: 2.0±0.2 Hz

Figure 2 continued on next page

Figure 2 continued

(*Atoh1^{Cre}*) and 1.4 ± 0.2 Hz (*Rapgef3;Rapgef4-cKO*; $p=0.0036$). Amplitude: 18.3 ± 1.3 pA (*Atoh1^{Cre}*) and 18.5 ± 1.3 pA (*Rapgef3;Rapgef4-cKO*; $p=0.46$). Unpaired *t* test. n =for all groups. $^{**}p<0.01$. (D) Example PC mEPSCs from *Prkce^{fl/fl}* and *Prkce-cKO* mice. Frequency: 1.9 ± 0.1 Hz (*Prkce^{fl/fl}*; $n=19$) and 1.3 ± 0.1 Hz (*Prkce-cKO*; $n=20$; $p=0.00059$). Amplitude: 17.9 ± 1.2 pA (*Prkce^{fl/fl}*; $n=19$) and 17.5 ± 1.1 pA (*Prkce-cKO*; $n=20$; $p=0.39$). Unpaired *t* test. $^{***}p<0.001$. (E) Representative responses of *Atoh1^{Cre}* and *Rapgef3;Rapgef4-cKO* PCs to 100 Hz PF stimulation. The artifacts were truncated and each EPSC were aligned to its initial rising point. RRP was defined as the y-intercept of linear portion of cumulative amplitude curve. For RRP (inset), *Atoh1^{Cre}*: 861 ± 113 ; *Rapgef3;Rapgef4-cKO*: 790 ± 101 ; $p=0.31$, unpaired *t* test. For cumulative amplitude, *Atoh1^{Cre}*: 5815 ± 360 pA; *Rapgef3;Rapgef4-cKO*: 3848 ± 66 pA; $p<0.001$, unpaired *t* test. For Pr, *Atoh1^{Cre}*: 0.17 ± 0.03 ; *Rapgef3;Rapgef4-cKO*: 0.11 ± 0.01 ; $p=0.043$, unpaired *t* test. $n=7$ for both groups. $^{*}p<0.05$. $^{***}p<0.001$. (F) Representative responses of *Prkce^{fl/fl}* and *Prkce-cKO* PCs to 100 Hz PF stimulation. The artifacts were truncated and each EPSC was aligned to its initial rising point. For RRP, *Prkce^{fl/fl}*, 764 ± 100 ; *Prkce-cKO*, 728 ± 106 , $p=0.40$, unpaired *t* test. For cumulative amplitude, *Prkce^{fl/fl}*, 5940 ± 337 pA; *Prkce-cKO*, 3755 ± 181 pA; $p<0.001$, unpaired *t* test. For Pr, *Prkce^{fl/fl}*, 0.19 ± 0.04 ; *Prkce-cKO*, 0.12 ± 0.01 ; $p=0.034$, unpaired *t* test. $n=7$ for both groups. $^{*}p<0.05$. $^{***}p<0.001$. (G) Cerebellar synaptosomes from WT and *Rapgef3/4-dKO* mice were immunoprecipitated by anti-RIM1 antibody, and the immunoprecipitates were probed with antibodies to Munc13-1, Rab3A, and RIM1. Rabbit IgG was negative control. Ratios of immunoprecipitated Munc13-1 or Rab3A vs. RIM1 were normalized to WT. Munc13-1: $100 \pm 6\%$ (WT) and $62 \pm 8\%$ (*Rapgef3/4-dKO*; $p=0.0081$, $n=4$). Rab3A: $100 \pm 5\%$ (WT) and $63 \pm 10\%$ (*Rapgef3/4-dKO*; $p=0.019$, $n=4$). Total Rab3A and RIM1 were normalized to WT. Munc13-1: $100 \pm 2\%$ (WT) and $98 \pm 4\%$ (*Rapgef3/4-dKO*; $p=0.73$, $n=6$). Rab3A: $100 \pm 5\%$ (WT) and $98 \pm 4\%$ (*Rapgef3/4-dKO*; $p=0.77$, $n=6$). Unpaired *t* test. $^{*}p<0.05$. $^{**}p<0.01$. (H) Immunoprecipitation of Munc13-1 and Rab3A with RIM1 in cerebellar synaptosomes from *Prkce^{fl/fl}* and *Prkce-cKO* mice. Ratios of immunoprecipitated Munc13-1 or Rab3A vs. RIM1 were normalized to WT. Munc13-1: $100 \pm 2\%$ (*Prkce^{fl/fl}*) and $70 \pm 8\%$ (*Prkce-cKO*; $p=0.0030$). Rab3A: $100 \pm 2\%$ (*Prkce^{fl/fl}*) and $89 \pm 4\%$ (*Prkce-cKO*; $p=0.019$). Total Rab3A and RIM1 were normalized to *Prkce^{fl/fl}*. Munc13-1: $100 \pm 3\%$ (*Prkce^{fl/fl}*) and $96 \pm 5\%$ (*Prkce-cKO*; $p=0.46$). Rab3A: $100 \pm 7\%$ (*Prkce^{fl/fl}*) and $106 \pm 5\%$ (*Prkce-cKO*; $p=0.52$). $n=6$ for all groups. Unpaired *t* test. $^{*}p<0.05$. $^{**}p<0.01$. (I) Cerebellar synaptosomes (WT) mice were incubated in control buffer or 8-pCPT (20 μ M, 30 min) and ϵ V1-2 (5 μ M, 30 min) and immunoprecipitated. Ratios of immunoprecipitated Munc13-1 or Rab3A vs. RIM1 were normalized to control. Munc13-1: $100 \pm 8\%$ (Ctrl); $138 \pm 12\%$ (8-pCPT; $p=0.041$ vs. Ctrl); $96 \pm 12\%$ (8-pCPT+ ϵ V1-2; $p=0.97$ vs. Ctrl; $p=0.029$ vs 8-pCPT). Rab3A: $100 \pm 5\%$ (Ctrl); $168 \pm 12\%$ (8-pCPT; $p=0.0011$ vs. Ctrl); $133 \pm 12\%$ (8-pCPT+ ϵ V1-2; $p=0.069$ vs. Ctrl; $p=0.046$ vs 8-pCPT). One-way ANOVA test. $n=4$ for all groups. $^{*}p<0.05$. $^{**}p<0.01$. (J) Cerebellar synaptosomes (WT) were treated with control buffer or FR236924 (FR) (200 nM, 30 min) and immunoprecipitated. Ratios of immunoprecipitated Munc13-1 or Rab3A vs. RIM1 were normalized to Ctrl. Munc13-1: $100 \pm 4\%$ (Ctrl) and $144 \pm 16\%$ (FR; $p=0.041$). Rab3A: $100 \pm 4\%$ (Ctrl) and $175 \pm 13\%$ (FR; $p=0.0016$). Unpaired *t* test. $n=4$ for all groups. $^{*}p<0.05$. $^{**}p<0.01$. (K) Cerebellar synaptosomes (*Prkce-cKO*) were treated with control buffer or FR236924 and immunoprecipitated. Ratios of immunoprecipitated Munc13-1 or Rab3A vs. RIM1 were normalized to *Prkce-cKO*. Munc13-1: $100 \pm 3\%$ (*Prkce-cKO*; $n=4$) and $100 \pm 12\%$ (*Prkce-cKO* +FR; $p=0.99$; $n=4$). Rab3A: $100 \pm 2\%$ (*Prkce-cKO*; $n=8$) and $108 \pm 9\%$ (*Prkce-cKO* +FR; $p=0.37$; $n=8$). Unpaired *t* test. See the online **Figure 2—source data 1** file for source data of western blots in this figure.

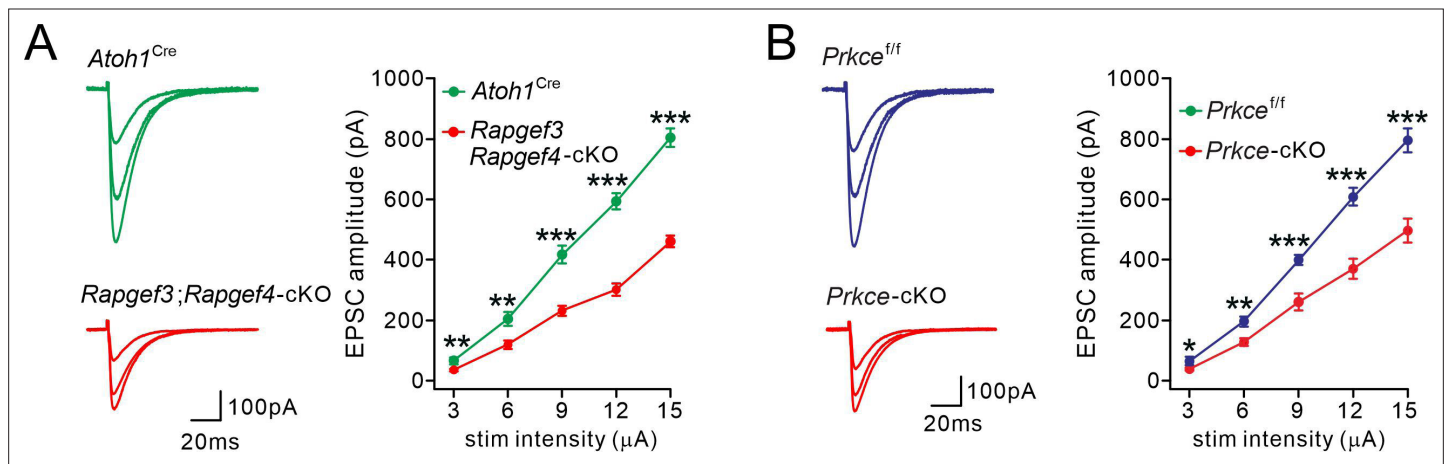


Figure 2—figure supplement 1. Input-output relationship of evoked PF-EPSCs in control and mutant mice. **(A)** Example PF-EPSCs obtained from *Atoh1^{Cre}* and *Rapgef3;Rapgef4-cKO* PCs with stimulation intensities of 6, 9, and 12 μ A. For *Atoh1^{Cre}* PCs, 66 ± 11 pA (3 μ A), 204 ± 23 pA (6 μ A); 417 ± 29 pA (9 μ A); 594 ± 26 pA (12 μ A); and 804 ± 32 pA (15 μ A); $n=9$. For *Rapgef3;Rapgef4-cKO* PCs, 36 ± 4 pA (3 μ A; $p=0.0034$), 119 ± 15 pA (6 μ A; $p=0.0022$); 231 ± 17 pA (9 μ A; $p<0.001$); 302 ± 20 pA (12 μ A; $p<0.001$); and 461 ± 19 pA (15 μ A; $p<0.001$); $n=10$. Unpaired *t* test. **(B)** Example PF-EPSCs obtained from *Prkce^{fl/fl}* and *Prkce-cKO* PCs with stimulation intensities of 6, 9, and 12 μ A. For *Prkce^{fl/fl}* PCs, 64 ± 14 pA (3 μ A), 196 ± 17 pA (6 μ A); 400 ± 17 pA (9 μ A); 608 ± 30 pA (12 μ A); and 796 ± 40 pA (15 μ A); $n=9$. For *Prkce-cKO* PCs, 39 ± 4 pA (3 μ A; $P=0.028$), 127 ± 12 pA (6 μ A; $p=0.001$); 260 ± 28 pA (9 μ A; $p=0.00011$); 370 ± 34 pA (12 μ A; $p<0.001$); and 497 ± 40 pA (15 μ A; $p<0.001$); $n=10$. Unpaired *t* test.

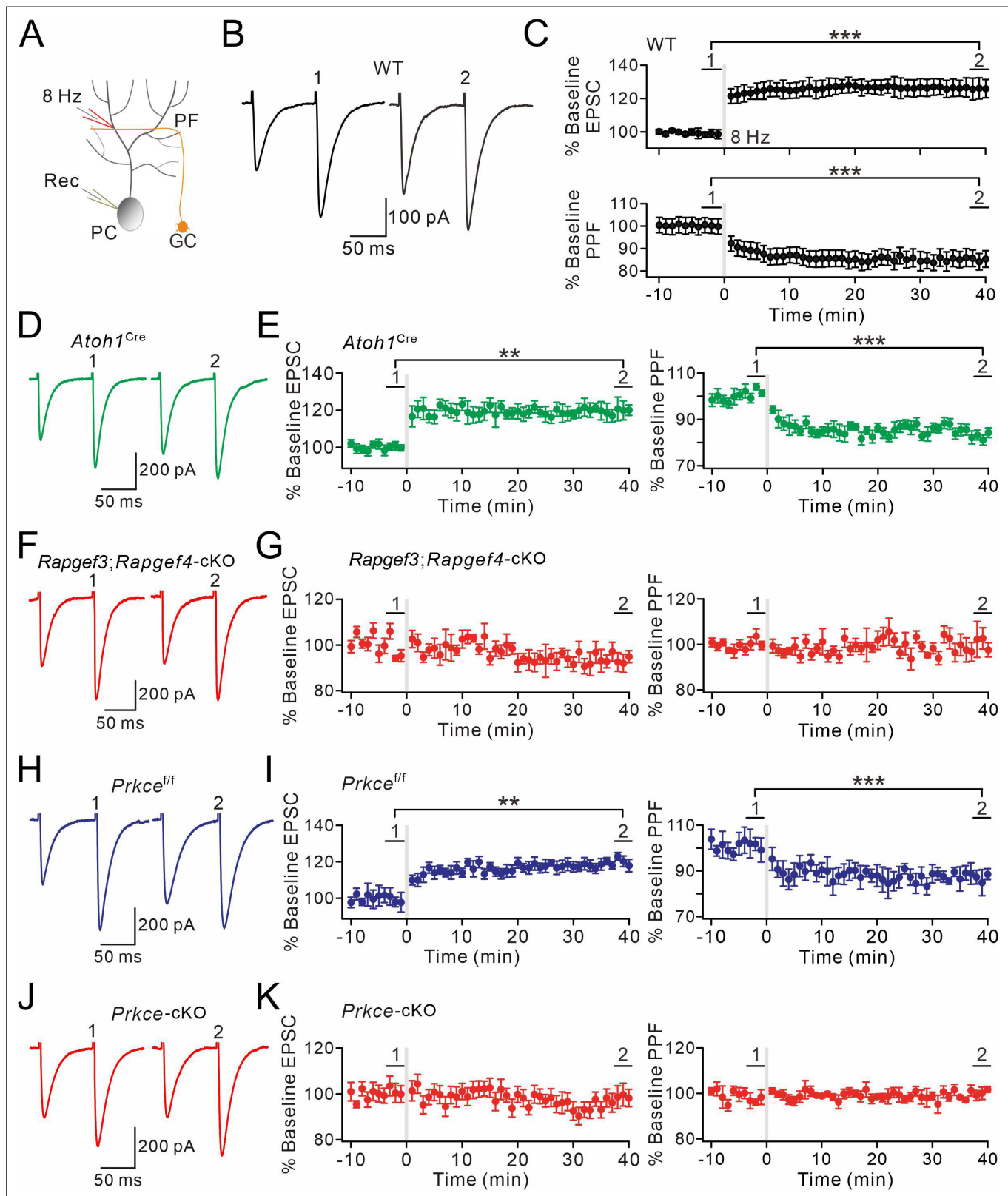


Figure 3. EPAC and PKC ϵ are required for presynaptic PF-LTP. (A) Schematic showing the induction of presynaptic LTP. (B, D, F, H, J) Example PF-EPSCs for baseline (1) and after LTP induction (2) in WT (B), *Atoh1^{Cre}* (D), *Rapgef3;Rapgef4-cKO* (F), *Prkce^{fl/fl}* (H), and *Prkce-cKO* (J) mice. (C) Percentage changes of PF-EPSC amplitudes (WT). (1): $101 \pm 4\%$; (2): $131 \pm 6\%$; $n=13$; $p<0.001$. Percentage changes of PPF ratios from cells shown above. (1): $101 \pm 3\%$; (2): $84 \pm 4\%$; $n=13$; $p<0.001$. Paired t test. *** $p<0.001$. (E) Left: percentage changes of PF-EPSC amplitudes (*Atoh1^{Cre}*). (1): $100 \pm 2\%$; (2): $120 \pm$

Figure 3 continued on next page

Figure 3 continued

5%; n=10; p=0.004. Right: percentage changes of PPF ratios. (1): $102 \pm 2\%$; (2): $83 \pm 2\%$; n=10; p<0.001. Unpaired t test. **p<0.01. ***p<0.001. **(G)** Left: percentage changes of PF-EPSC amplitudes (*Rapgef3;Rapgef4*-cKO). (1): $99 \pm 2\%$; (2): $93 \pm 4\%$; n=9; p=0.059. Right: percentage changes of PPF ratios. (1): $101 \pm 3\%$; (2): $101 \pm 5\%$; n=9; p=0.07. Paired t test. **(I)** Left: percentage changes of PF-EPSC amplitudes (*Prkce^{fl/y}*). (1): $99 \pm 4\%$; (2): $120 \pm 3\%$; n=7; p=0.004. Right: percentage changes of PPF ratios. (1): $100 \pm 5\%$; (2): $86 \pm 4\%$; n=7; p<0.001. Paired t test. **p<0.01. ***p<0.001. **(K)** Left: percentage changes of PF-EPSC amplitudes (*Prkce*-cKO). (1): $101 \pm 4\%$; (2): $99 \pm 5\%$; n=10; p=0.065. Right: percentage changes of PPF ratios. (1): $101 \pm 3\%$; (2): $100 \pm 2\%$; n=10; p=0.77. Paired t test.

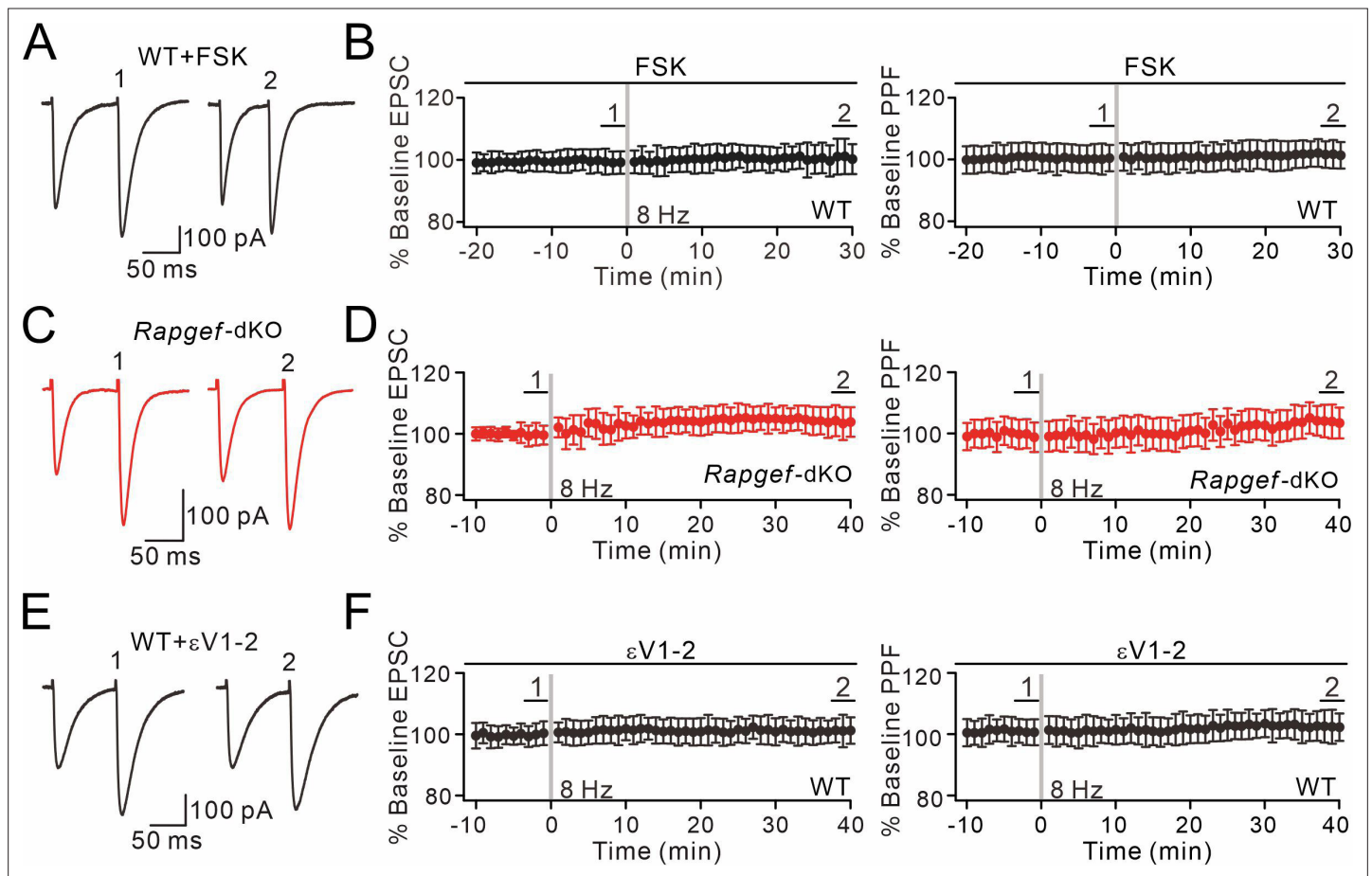


Figure 3—figure supplement 1. Presynaptic PF-PC LTP is blocked by forskolin incubation, EPAC ablation, or ϵ V1-2 application. **(A)** Example PF-EPSCs for baseline (1) and after LTP induction (2) in a WT PC perfused with forskolin (20 μ M). **(B)** Percentage changes of PF-EPSC amplitude with forskolin treatment in WT mice: 99 \pm 3% (1) and 101 \pm 5% (2); $n=11$; $p=0.63$. PPF ratios from cells shown in the left panel: 100 \pm 5% (1) and 102 \pm 4% (2); $n=11$; $p=0.72$. Paired t test. **(C)** Example PF-EPSCs for baseline and after LTP induction in an *Rapgef3/4*-dKO PC. **(D)** Percentage changes of PF-EPSC amplitude in *Rapgef3/4*-dKO mice: 100 \pm 3% (1) and 104 \pm 5% (2); $n=11$; $p=0.66$. PPF ratios from cells shown in the left panel: 99 \pm 5% (1) and 104 \pm 5% (2); $n=11$; $p=0.58$. Paired t test. **(E)** Example PF-EPSCs for baseline and after LTP induction in a WT PC perfused with ϵ V1-2 (5 μ M). **(F)** Percentage changes of PF-EPSC amplitude in WT mice: 100 \pm 3% (1) and 101 \pm 4% (2); $n=9$; $p=0.59$. PPF ratios from cells shown in the left panel: 101 \pm 4% (1) and 102 \pm 5% (2); $n=9$; $p=0.22$. Paired t test.

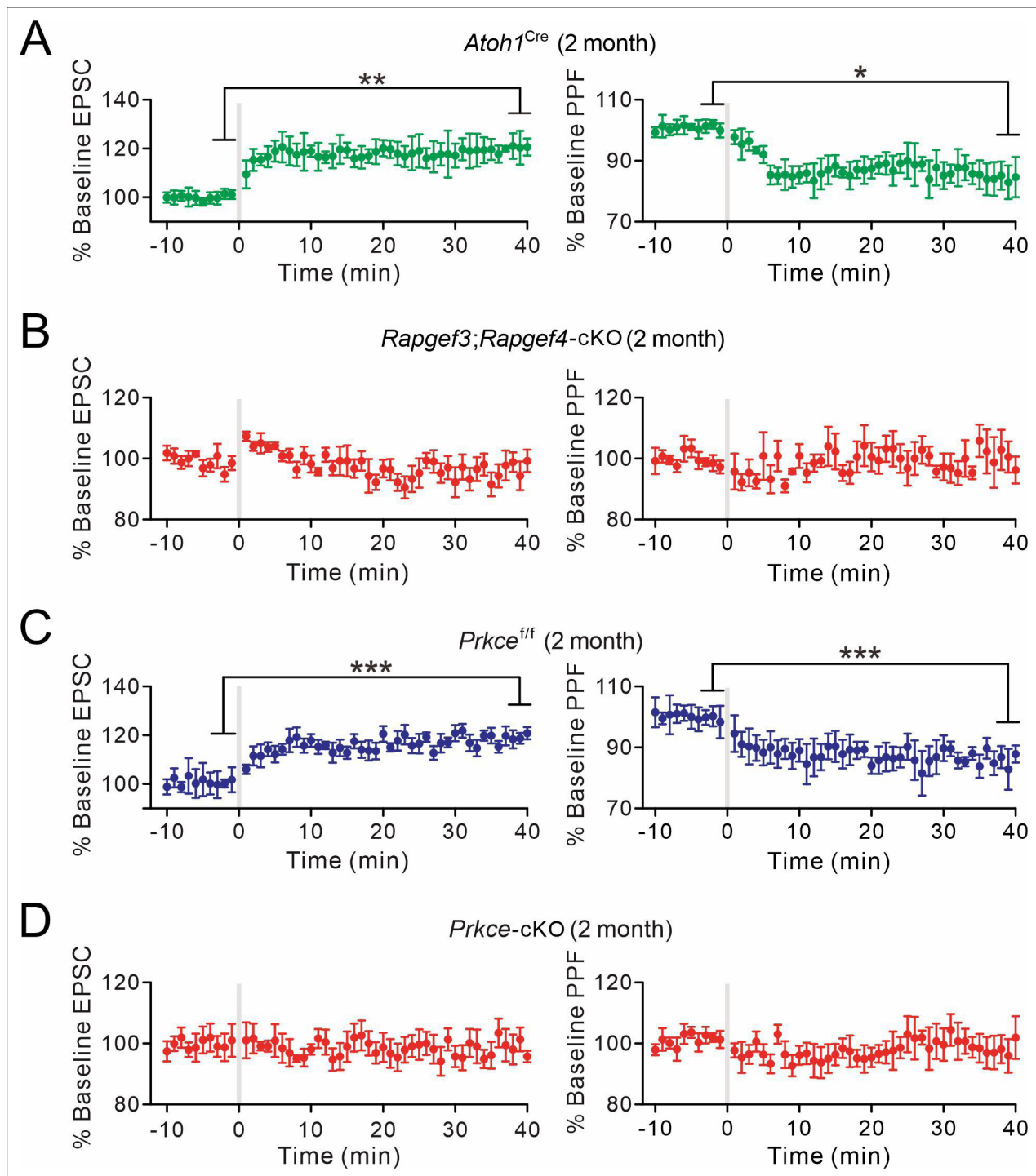


Figure 3—figure supplement 2. The induction of presynaptic PF-PC LTP in 2-month-old mice. (A) Left: percentage changes of PF-EPSC amplitudes (*Atoh1^{Cre}*). Right: percentage changes of PPF ratios. $84 \pm 4\%$ at $t=38-40$ min; $n=7$; $p=0.011$. Paired *t* test. * $p<0.05$. ** $p<0.01$. (B) Left: percentage changes of PF-EPSC amplitudes (*Rapgef3;Rapgef4-cKO*). Right: percentage changes of PPF ratios. $100 \pm 4\%$ at $t=38-40$ min; $n=6$; $p=0.97$. Paired *t* test. (C) Left: percentage changes of PF-EPSC amplitudes (*Prkce^{fl/fl}*). Right: percentage changes of PPF ratios. $86 \pm 2\%$ at $t=38-40$ min; $n=6$; $p=0.0008$. Paired *t* test. *** $p<0.001$. (D) Left: percentage changes of PF-EPSC amplitudes (*Prkce-cKO*). Right: percentage changes of PPF ratios. $99 \pm 5\%$ at $t=38-40$ min; $n=7$; $p=0.78$. Paired *t* test.

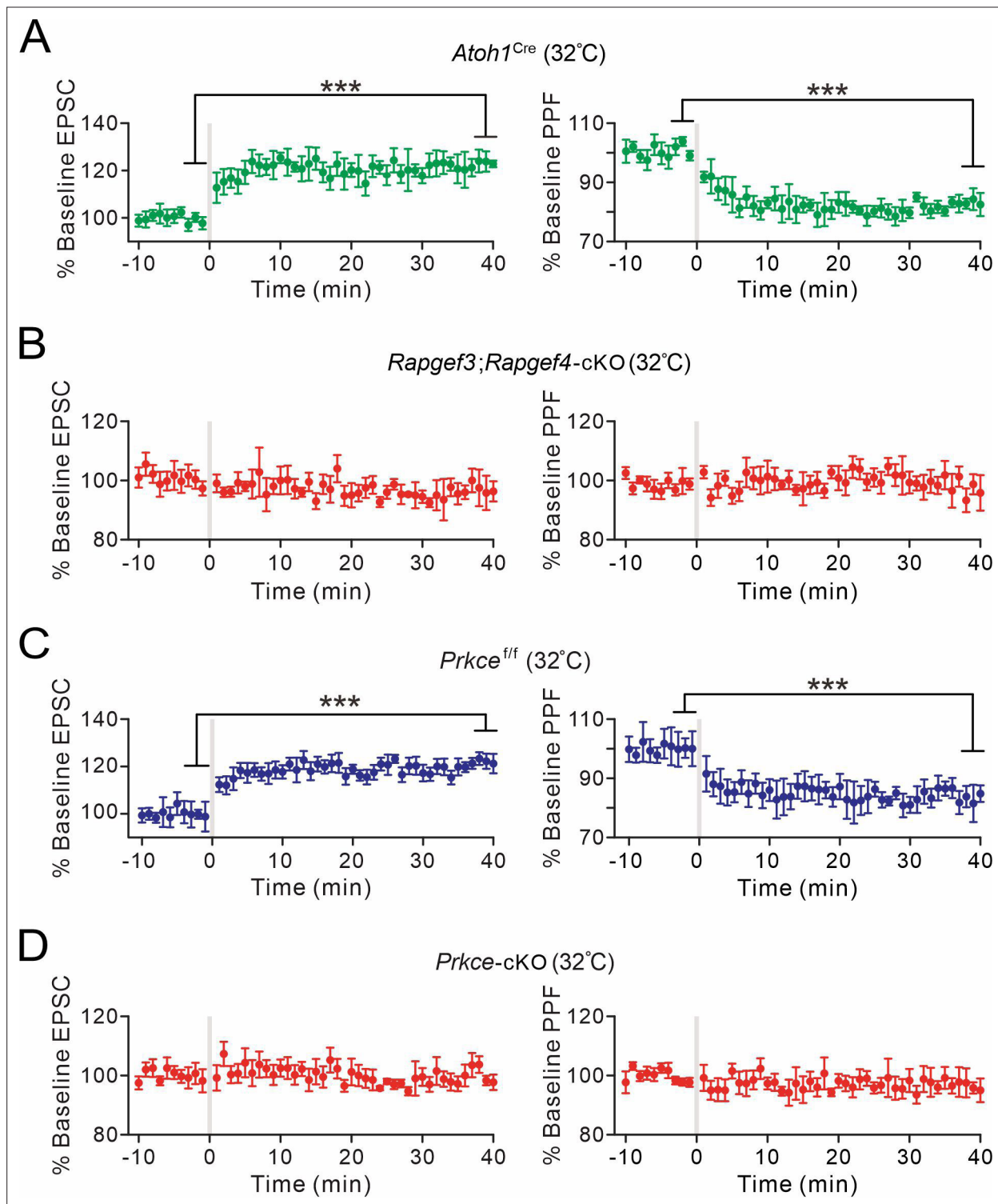


Figure 3—figure supplement 3. The induction of presynaptic PF-PC LTP in elevated temperature. (A) Left: percentage changes of PF-EPSC amplitudes (*Atoh1^{Cre}*). Right: percentage changes of PPF ratios. $83 \pm 2\%$ at $t=38-40$ min; $n=6$; $p=0.00036$. Paired t test. *** $p<0.001$. (B) Left: percentage changes of PF-EPSC amplitudes (*Rapgef3;Rapgef4-cKO*). Right: percentage changes of PPF ratios. $96 \pm 3\%$ at $t=38-40$ min; $n=6$; $p=0.27$. Paired t test. (C) Left: percentage changes of PF-EPSC amplitudes (*Prkce^{f/f}*). Right: percentage changes of PPF ratios. $83 \pm 2\%$ at $t=38-40$ min; $n=6$; $p=0.00039$. Paired t test. *** $p<0.001$. (D) Left: percentage changes of PF-EPSC amplitudes (*Prkce-cKO*). Right: percentage changes of PPF ratios. $96 \pm 3\%$ at $t=38-40$ min; $n=6$; $p=0.22$. Paired t test.

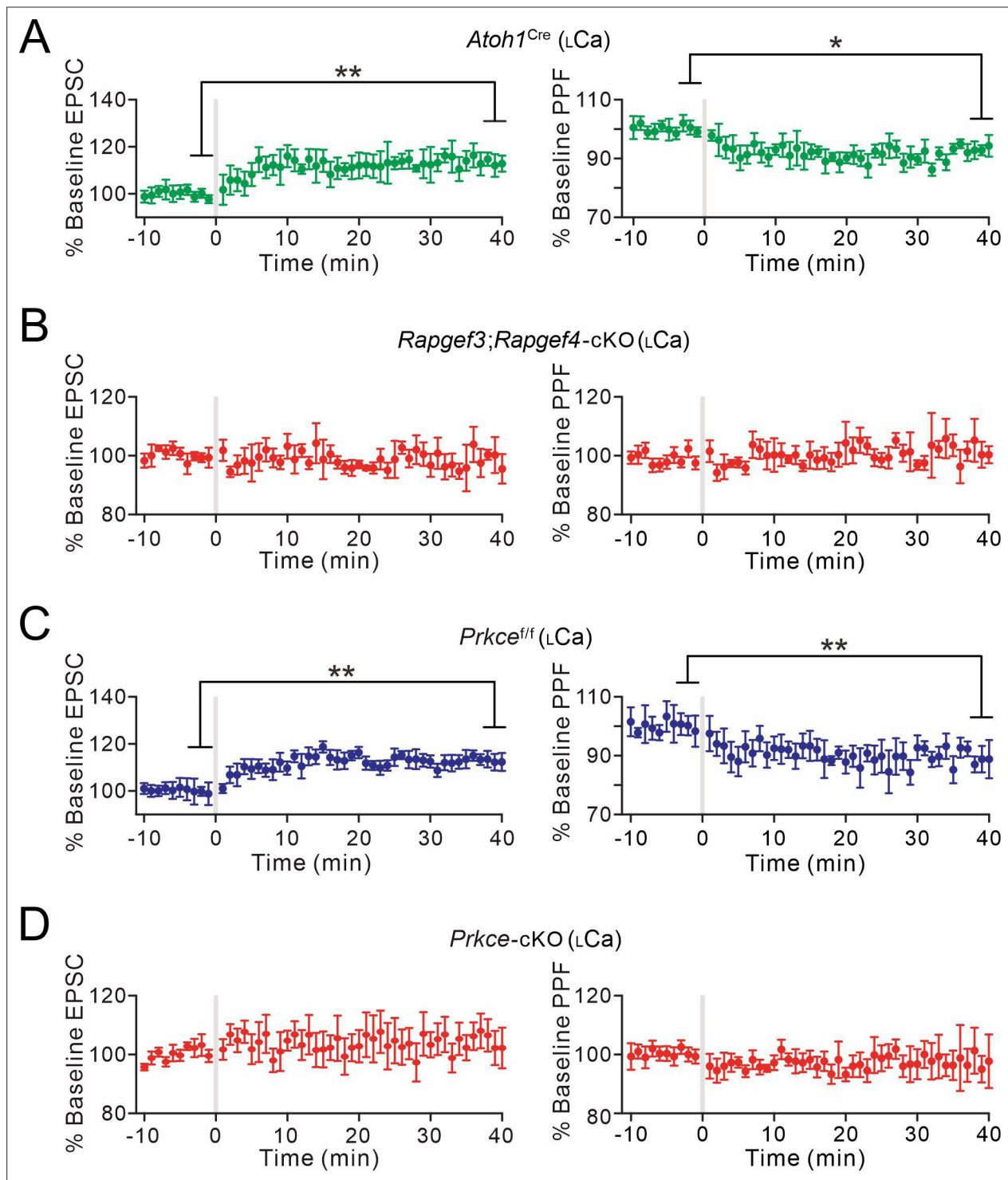


Figure 3—figure supplement 4. The induction of presynaptic PF-PC LTP in lower Ca^{2+} concentration. (A) Left: percentage changes of PF-EPSC amplitudes (*Atoh1^{Cre}*). Right: percentage changes of PPF ratios. $93 \pm 2\%$ at $t=38-40$ min; $n=6$; $p=0.017$. Paired t test. $*p<0.05$. $**p<0.01$. (B) Left: percentage changes of PF-EPSC amplitudes (*Rapgef3;Rapgef4-cKO*). Right: percentage changes of PPF ratios. $102 \pm 2\%$ at $t=38-40$ min; $n=6$; $p=0.42$. Paired t test. (C) Left: percentage changes of PF-EPSC amplitudes (*Prkce^{flf}*). Right: percentage changes of PPF ratios. $88 \pm 6\%$ at $t=38-40$ min; $n=6$; $p=0.005$. Paired t test. $**p<0.01$. (D) Left: percentage changes of PF-EPSC amplitudes (*Prkce-cKO*). Right: percentage changes of PPF ratios. $98 \pm 2\%$ at $t=38-40$ min; $n=6$; $p=0.76$. Paired t test.

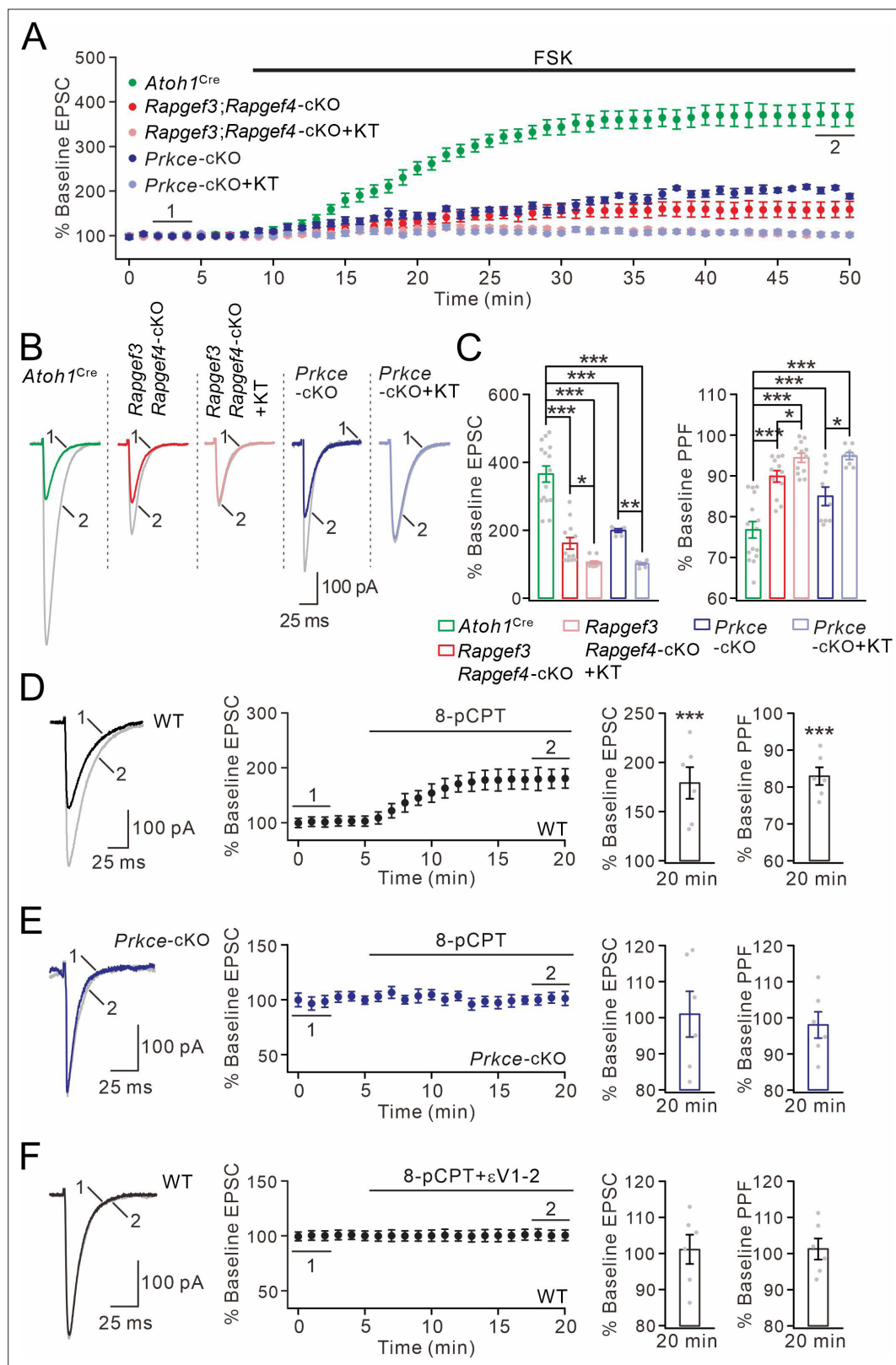


Figure 4. cAMP-triggered PF facilitation is dependent on EPAC and PKC ϵ . **(A)** The facilitation of PF-EPSCs by forskolin (FSK) (20 μ M) in *Atoh1*^{Cre}, *Rapgef3*;*Rapgef4*-cKO and *Prkce*-cKO mice. **(B)** Example traces for baseline (1) and after potentiation (2) shown in **(A)**. **(C)** Left: percent changes of EPSC amplitude. *Atoh1*^{Cre}: 366 \pm 25% (n=15); *Rapgef3*;*Rapgef4*-cKO: 162 \pm 18% (n=12; p<0.001 vs. *Atoh1*^{Cre}); *Rapgef3*;*Rapgef4*-cKO+KT: 106 \pm 4% (n=12;

Figure 4 continued on next page

Figure 4 continued

$p < 0.001$ vs. *Atoh1^{Cre}*; $p = 0.046$ vs. *Rapgef3;Rapgef4-cKO*; *Prkce-cKO*: $198 \pm 5\%$ ($n = 12$; $p < 0.001$ vs. *Atoh1^{Cre}*); *Prkce-cKO* + KT: $101 \pm 3\%$ ($n = 12$; $p < 0.001$ vs. *Atoh1^{Cre}*; $p = 0.0034$ vs. *Prkce-cKO*). Right: percent changes of PPF. *Atoh1^{Cre}*: $77 \pm 2\%$ ($n = 15$); *Rapgef3;Rapgef4-cKO*: $90 \pm 1\%$ ($n = 12$; $p < 0.001$ vs. *Atoh1^{Cre}*); *Rapgef3;Rapgef4-cKO* + KT: $94 \pm 1\%$ ($n = 12$; $p < 0.001$ vs. *Atoh1^{Cre}*; $p = 0.049$ vs. *Rapgef3;Rapgef4-cKO*); *Prkce-cKO*: $85 \pm 2\%$ ($n = 12$; $p < 0.001$ vs. *Atoh1^{Cre}*); *Prkce-cKO* + KT: $95 \pm 1\%$ ($n = 12$; $p < 0.001$ vs. *Atoh1^{Cre}*; $p = 0.025$ vs. *Prkce-cKO*). One-way ANOVA test. * $p < 0.05$. *** $p < 0.001$. (D) Bath application of 8-pCPT (20 μ M) caused PF-EPSC potentiation in WT mice. Left: example traces before (1) and after potentiation (2). Middle: time course of PF facilitation. Right: percent changes of EPSC amplitude ($179 \pm 18\%$; $n = 6$; $p < 0.001$) and PPF ($83 \pm 3\%$; $n = 6$; $p < 0.001$) at 18–20 min vs. baseline (0–2 min). Paired *t* test. *** $p < 0.001$. (E) 8-pCPT failed to induce PF-EPSC potentiation in *Prkce-cKO* mice. Left: example traces for baseline (1) and after potentiation (2). Middle: time course of PF facilitation. Right: percent changes of EPSC amplitude ($101 \pm 6\%$; $n = 6$; $p = 0.35$) and PPF ($98 \pm 4\%$; $n = 6$; $p = 0.45$) at 18–20 min vs. baseline (0–2 min). Paired *t* test. (F) Co-application of 8-pCPT and ϵ V1-2 (5 μ M) failed to produce PF potentiation in WT mice. Left: example traces for baseline (1) and after potentiation (2). Middle: time course of PF-EPSCs. Right: percent changes of EPSC amplitude ($101 \pm 4\%$; $n = 6$; $p = 0.78$) and PPF ($101 \pm 3\%$; $n = 6$; $p = 0.67$) at 18–20 min vs. baseline (0–2 min). Paired *t* test.

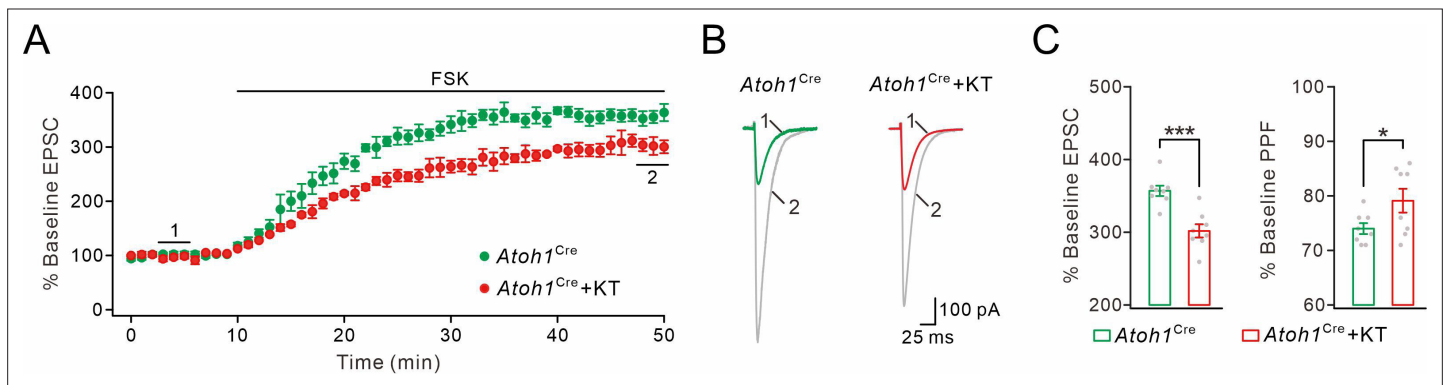


Figure 4—figure supplement 1. PKA inhibition has a modest effect in blocking cAMP-triggered facilitation. **(A)** The facilitation of PF-EPSCs by forskolin (FSK) (20 μ M) and its inhibition by KT5720 (3 μ M) in *Atoh1^{Cre}* mice. **(B)** Example traces for baseline (1) and after potentiation (2) shown in **(A)**. **(C)** Left: percent changes of EPSC amplitude. *Atoh1^{Cre}*: $357 \pm 8\%$ (n=8); *Atoh1^{Cre}+KT5720*: $302 \pm 10\%$ (n=8; p=0.00015). Right: percent changes of PPF. *Atoh1^{Cre}*: $74 \pm 1\%$ (n=8); *Atoh1^{Cre}+KT5720*: $79 \pm 2\%$ (n=8; p=0.026). Paired t test. *p<0.05. ***p<0.001.

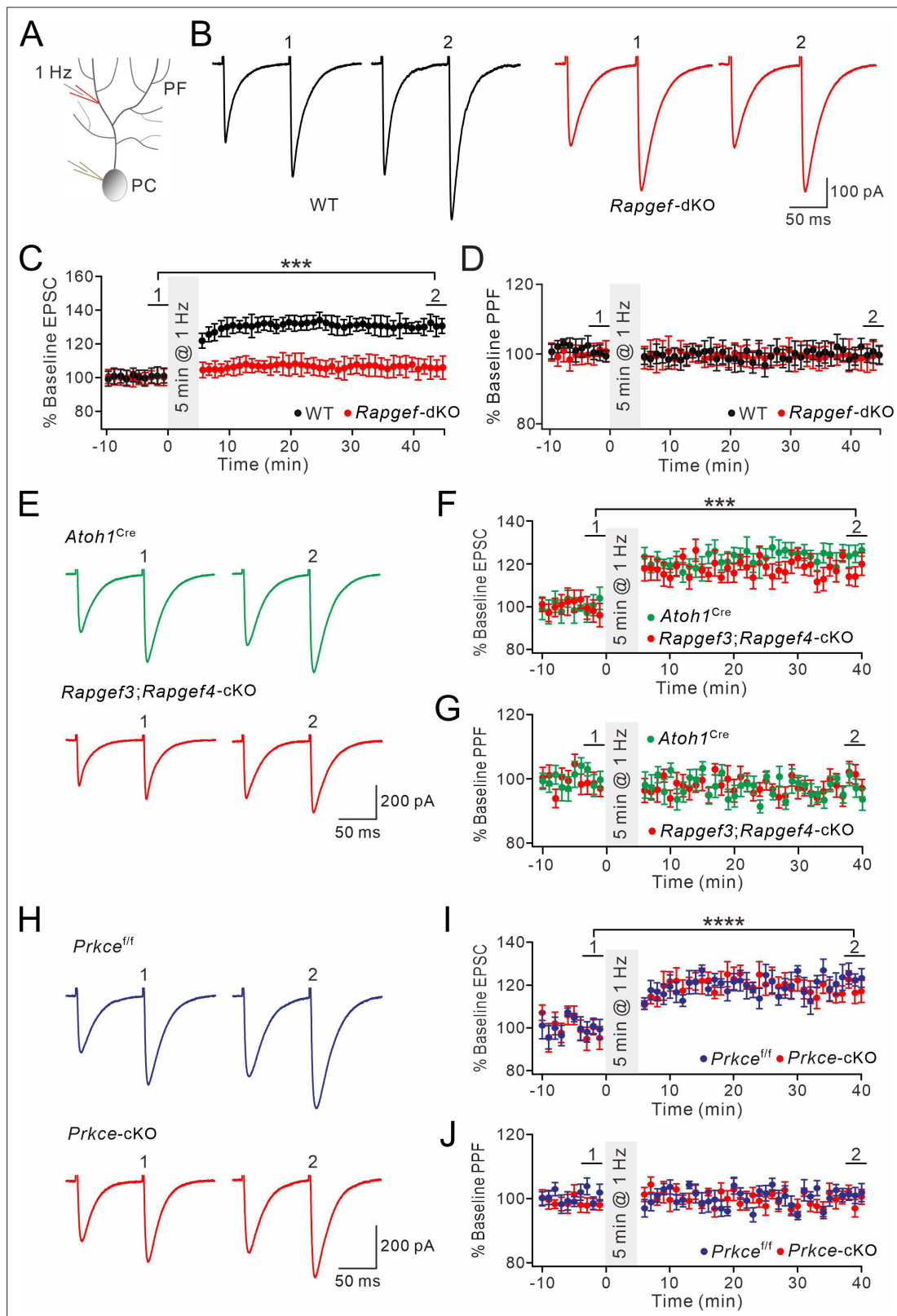


Figure 5. Postsynaptic PF-PC LTP is intact upon presynaptic deletion of EPAC or PKC ϵ . (A) Schematic showing the induction of postsynaptic LTP. (B, E, H) Example PF-EPSCs for baseline (1) and after induction (2) in WT and *Rapgef3/4*-dKO PCs (B), *Atoh1*^{Cre} and *Rapgef3/4*-cKO PCs (E), and *Prkce*^{f/f} and *Prkce*-cKO PCs (H). (C) Percentage changes of PF-EPSC amplitude. In WT, 101 ± 5% for (1) and 131 ± 5% for (2) ($p < 0.001$). In *Rapgef3/4*-dKO, 100 ± 5% for (1) and 106 ± 6% for (2) ($p = 0.26$). Paired t test. $n = 13$ for both groups. *** $p < 0.001$. (D) Percentage changes of PPF ratios of cells shown in (C). In

Figure 5 continued on next page

Figure 5 continued

WT, $100 \pm 2\%$ for (1) and $100 \pm 3\%$ for (2) ($p=0.63$). In *Rapgef3/4*-dKO, $101 \pm 3\%$ for (1) and $99 \pm 4\%$ for (2) ($p=0.74$). Paired t test. $n=13$ for both groups. **(F)** Percentage changes of PF-EPSC amplitude. In *Atoh1*^{Cre}, $100 \pm 5\%$ for (1) and $123 \pm 3\%$ for (2) ($p<0.001$). In *Rapgef3;Rapgef4*-cKO, $98 \pm 5\%$ for (1) and $119 \pm 4\%$ for (2) ($p<0.001$). Paired t test. $n=7$ for both groups. *** $p<0.001$. **(G)** Percentage changes of PPF ratios of cells shown in **(C)**. In *Atoh1*^{Cre}: $100 \pm 2\%$ for (1) and $96 \pm 3\%$ for (2) ($p=0.26$). In *Rapgef3;Rapgef4*-cKO: $98 \pm 3\%$ for (1) and $95 \pm 3\%$ for (2) ($p=0.28$). Paired t test. $n=7$ for both groups. **(I)** Percentage changes of PF-EPSC amplitude. In *Prkce*^{if}, $99 \pm 4\%$ for (1) and $121 \pm 4\%$ for (2) ($p<0.0001$). In *Prkce*-cKO: $97 \pm 5\%$ for (1) and $118 \pm 5\%$ for (2) ($p<0.0001$). Paired t test. $n=7$ for both groups. **** $p<0.0001$. **(J)** Percentage changes of PPF ratios from cells shown in **(I)**. In *Prkce*^{if}, $102 \pm 2\%$ for (1) and $101 \pm 2\%$ for (2) ($p=0.73$). In *Prkce*-cKO, $98 \pm 2\%$ and $100 \pm 2\%$ for (2) ($p=0.78$). Paired t test. $n=7$ for both groups.

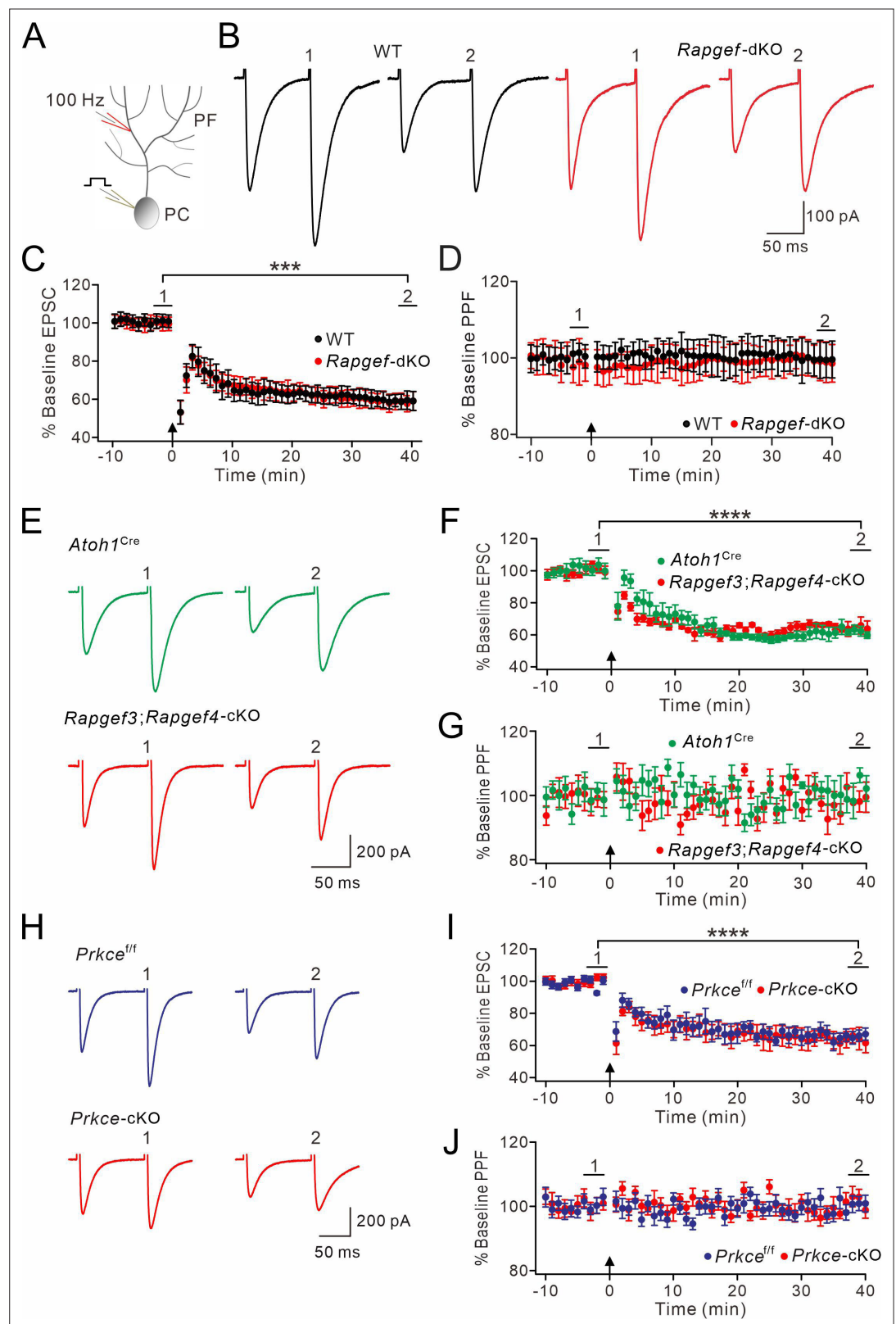


Figure 6. PF-LTD is unaltered by presynaptic deletion of EPAC or PKC ϵ . (A) A scheme showing the induction of postsynaptic LTD. (B, E, H) Example PF-EPSCs for baseline (1) and after LTD induction (2) in WT and *Rapgef3/4*-dKO PCs (B), *Atoh1*^{Cre} and *Rapgef3/4*-cKO PCs (E), and *Prkce*^{f/f} and *Prkce*-cKO PCs (H). (C) Percentage changes of PF-EPSC amplitude. In WT, $101 \pm 3\%$ for (1) and $59 \pm 5\%$ for (2) ($p < 0.001$). In *Rapgef3/4*-dKO, $100 \pm 3\%$

Figure 6 continued on next page

Figure 6 continued

for (1) and $59 \pm 4\%$ for (2) ($p < 0.001$). Paired *t* test. $n=13$ for both groups. *** $p < 0.001$. (D) Percentage changes of PPF ratios of cells shown in (C). In WT, $100 \pm 3\%$ for (1) and $100 \pm 5\%$ for (2) ($p=0.49$). In *Rapgef3/4*-dKO, $100 \pm 5\%$ for (1) and $100 \pm 5\%$ for (2) ($p=0.26$). Paired *t* test. $n=13$ for both groups. (F) Percentage changes of PF-EPSC amplitude. In *Atoh1^{Cre}*, $100 \pm 4\%$ for (1) and $61 \pm 3\%$ for (2) ($p < 0.0001$). In *Rapgef3;Rapgef4*-cKO, $101 \pm 3\%$ for (1) and $65 \pm 4\%$ for (2) ($p < 0.0001$). Paired *t* test. $n=7$ for both groups. **** $p < 0.0001$. (G) Percentage changes of PPF ratios of cells shown in (F). In *Atoh1^{Cre}*, $100 \pm 2\%$ for (1) and $100 \pm 3\%$ for (2) ($p=0.40$). In *Rapgef3;Rapgef4*-cKO, $101 \pm 3\%$ for (1) and $99 \pm 4\%$ for (2) ($p=0.61$). Paired *t* test. $n=7$ for both groups. (I) Percentage changes of PF-EPSC amplitude. In *Prkce^{fl}*, $99 \pm 2\%$ for (1) and $66 \pm 4\%$ for (2) ($p < 0.0001$). In *Prkce*-cKO, baseline: $101 \pm 2\%$ for (1) and $64 \pm 6\%$ for (2) ($p < 0.0001$). Paired *t* test. $n=7$ for both groups. **** $p < 0.0001$. (J) Percentage changes of PPF ratios of cells shown in (I). In *Prkce^{fl}*, $101 \pm 2\%$ for (1) and $101 \pm 2\%$ for (2) ($p=0.56$). In *Prkce*-cKO, $100 \pm 2\%$ for (1) and $102 \pm 2\%$ for (2) ($p=0.54$). Paired *t* test. $n=7$ for both groups.

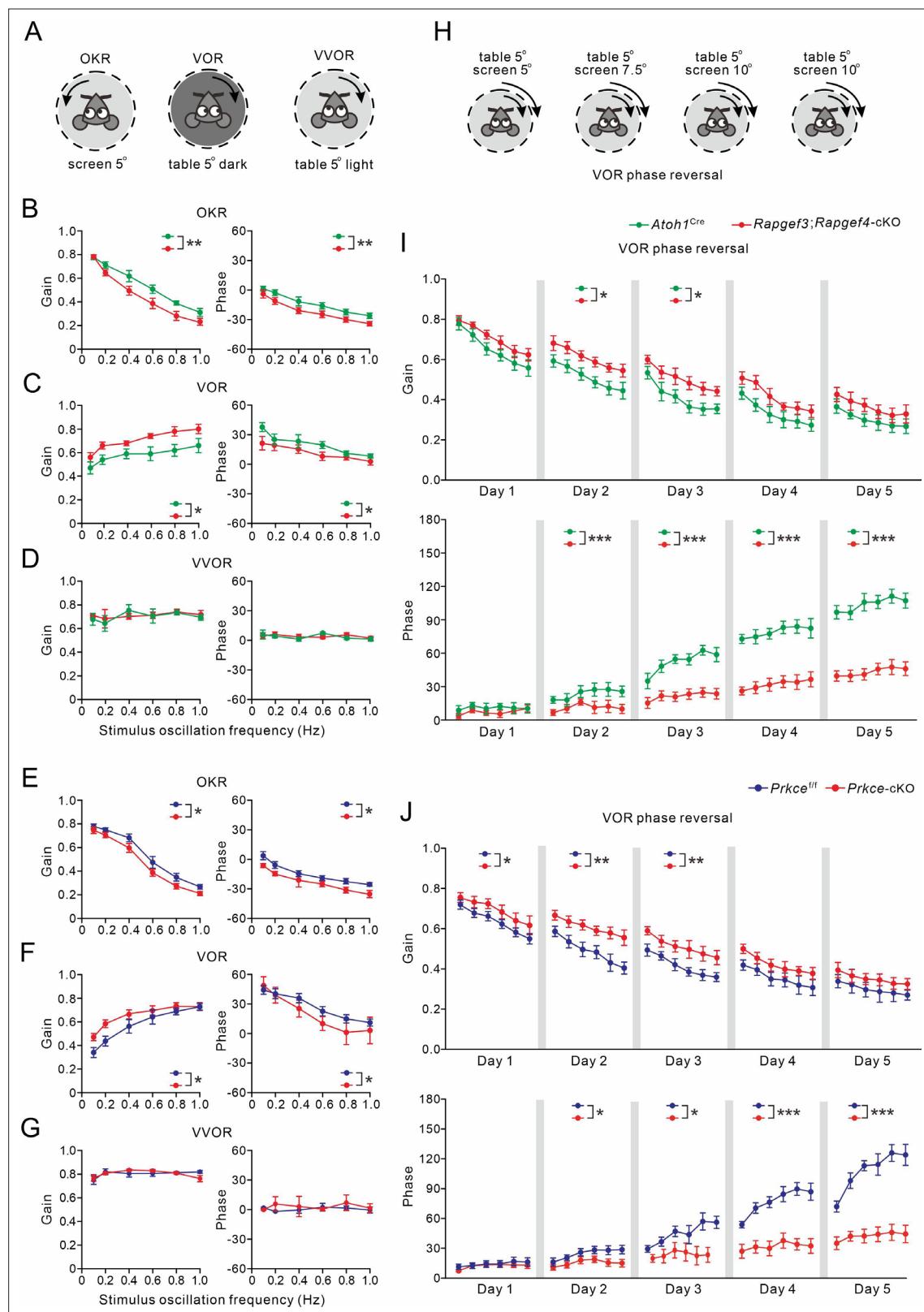


Figure 7. VOR baseline and adaptation in *Atoh1^{Cre}*, *Rapgef3;Rapgef4-cKO*, *Prkce^{fl/fl}* and *Prkce-cKO* mice. (A) Pictograms depicted compensatory eye movements driven by visual stimulus (OKR), vestibular stimulus (VOR) or both (VVOR). (B) OKR gain (measure of eye movement amplitude) and phase (measure of timing) were smaller in *Rapgef3;Rapgef4-cKO* ($n=16$) mice compared to *Atoh1^{Cre}* ($n=10$) mice. (C) VOR was affected in *Rapgef3;Rapgef4-cKO* mice. (D) The combination of vestibular and visual input by rotation of the mouse in the light evoked the VVOR in *Atoh1^{Cre}* and *Rapgef3;Rapgef4-cKO* mice. Figure 7 continued on next page

Figure 7 continued

cKO mice. (E) OKR gain and phase were smaller in *Prkce*-cKO (n=11) mice compared to *Prkce*^{+/f} (n=10) mice. (F) VOR was affected in *Prkce*-cKO mice. (G) VVOR gain and phase in *Prkce*^{+/f} and *Prkce*-cKO mice. (H) Mismatched visual and vestibular input was used to trigger adaptation of the eye movements in order to test motor learning ability. This training induced a reversal of VOR phase probed by VOR recordings in the dark. (I) Both gain-decrease learning and phase learning of *Rapgef3;Rapgef4*-cKO were impaired. * $p < 0.05$. *** $p < 0.001$. (J) Both gain-decrease learning and phase learning of *Prkce*-cKO were impaired. * $p < 0.05$. ** $p < 0.01$. *** $p < 0.001$.

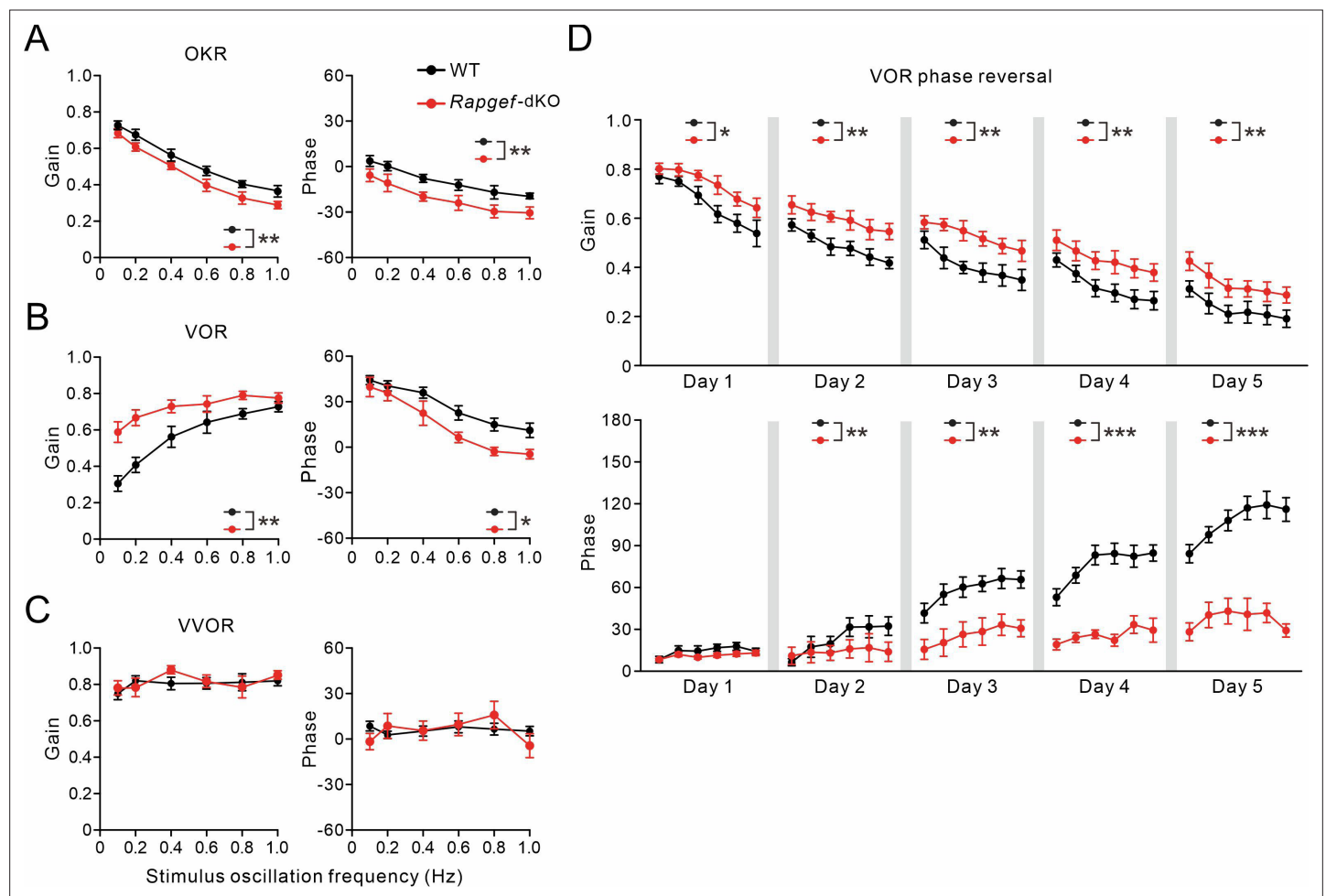


Figure 7—figure supplement 1. Impaired VOR learning in *Rapgef3/4*-dKO mice. **(A)** Gain and phase values of WT ($n=10$) and *Rapgef3/4*^{dKO} ($n=10$) mice during OKR evoked by visual stimulation. ** $p<0.01$. **(B)** Gain and phase values of WT and *Rapgef3/4*^{dKO} mice evoked by vestibular stimulation in the dark. * $p<0.05$. ** $p<0.01$. **(C)** Gain and phase values of WT and *Rapgef3/4*-dKO mice during VVOR in the light. With visual input, the VOR deficits in *Rapgef3/4*-dKO were no longer present. **(D)** VOR recordings in the dark revealed a reversal of VOR phase in WT and *Rapgef3/4*-dKO mice. * $p<0.05$. ** $p<0.01$. *** $p<0.001$.

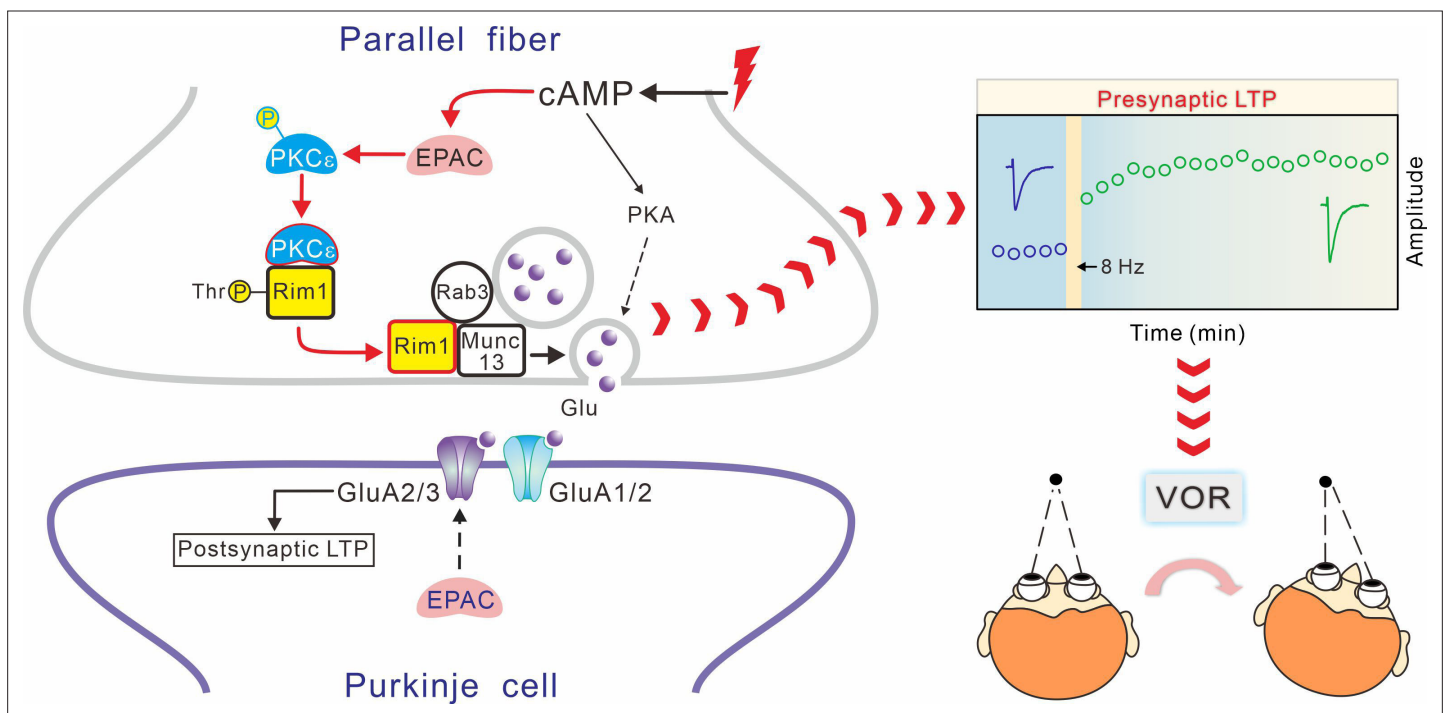


Figure 7—figure supplement 2. Proposed schematic model for the function of EPAC-PKCε module in presynaptic LTP and motor learning. In this model, EPAC activation by forskolin or presynaptic tetanus stimulation promotes PKCε activation and phosphorylation threonine of RIM1, which further facilitates the assembly of Rab3A-RIM1-Munc13-1 tripartite complex and the docking of vesicles at active zones. All these events are required for the induction of presynaptic LTP. Importantly, presynaptic LTP is essential to VOR phase adaptation learning.